applied sciences

MDPI

Article

Tribological Properties and Seasonal Freezing Damage Evolution of Rotating Spherical Hinge Self-Lubricating Coating

Wenting Dai [1,*], Jinghao Zuo [2], Dehao Liu [2] and Xuedong Guo [2]

[1] College of Construction Engineering, Jilin University, Changchun 130022, China
[2] College of Transportation, Jilin University, Changchun 130022, China
* Correspondence: daiwt@jlu.edu.cn; Tel.: +86-130-8681-4298

Featured Application: This paper will provide a theoretical basis for the selection of spherical hinge lubrication materials for rotary bridges and promote the research and development of lubricants for rotary bridges under special conditions.

Abstract: The spherical hinge is an important part of rotating bridge construction, but over a long period of time, spherical hinge self-lubricating coating is easily eroded by water vapor. In this paper, the tribological properties and seasonal freezing damage evolution characteristics of a variety of rotating spherical hinge self-lubricating coating materials were studied by means of friction coefficient measurement experiments, friction and wear experiments and shear rheological experiments based on a self-developed indoor spherical hinge rotational friction coefficient tester. The results show that the self-developed indoor spherical hinge rotational friction coefficient tester can effectively and truly represent the working state and tribological properties of self-lubricating coating in practical engineering. A seasonal freezing environment has obvious influence on the tribological properties of spherical hinge self-lubricating coating, which is an irreversible process of deterioration. With the increase in the freezing–thawing cycle, the friction coefficient and viscosity of self-lubricating coating materials increase gradually, and the thixotropy and elastic recovery become worse and worse. When the content of graphene is 0.1%, the performance is the best. At room temperature and in a freeze–thaw environment, the friction coefficient of graphene grease is lower than that of PTFE 0.007 and 0.008, respectively. The diameter of the grinding plate is less than 0.075 mm and 0.001 mm, respectively. The maximum bite load without card is higher than 8.1% and 11.5%. The area of the thixotropic ring is lower than 41% and 42%. Phase transition points were higher than 42% and 64%. The apparent viscosity was higher than 6.6% and 74%. Graphene greases show the greatest bearing capacity, thixotropy and structural strength in conventional and seasonal freezing conditions and exhibit excellent tribological properties.

Keywords: rotation construction; spherical hinge structure; self-lubricating coating; tribological properties; season frozen damage

Citation: Dai, W.; Zuo, J.; Liu, D.; Guo, X. Tribological Properties and Seasonal Freezing Damage Evolution of Rotating Spherical Hinge Self-Lubricating Coating. *Appl. Sci.* **2022**, *12*, 8329. https://doi.org/10.3390/app12168329

Academic Editor: Luís Picado Santos

Received: 27 June 2022
Accepted: 18 August 2022
Published: 20 August 2022

1. Introduction

Bridge rotation construction is new bridge construction technology developed in the middle of the last century. It refers to a construction method in which the bridge structure is cast or assembled at the non-designed axis and rotated to the designed axis through a rotation system [1–4]. Compared with the traditional bridge beam construction method, the swivel bridge has the advantages of not being restricted by the site, not affecting the traffic navigation under the bridge, fast construction speed and low cost [5,6]. The swivel bridge is mainly composed of the superstructure, the spherical hinge structure, the substructure and the traction device, including spherical hinge structure. This is the most critical core component in the swivel bridge, and it is also a typical component that is different from the conventional bridge. Its main functions in the construction process include core load, balance control and rotation control [7,8].

The weight of the whole swivel bridge will be transmitted to the lower turntable through the spherical hinge, and the size of the rotational friction coefficient will directly affect the size of the rotational moment required for traction and whether the rotation is successful [9]. Although friction cannot be avoided, it can be reduced by changing the slider material or adding grease [10]. Grease is applied between the upper and lower turntables of the spherical hinge. As the spherical hinge is squeezed by the superstructure and the substructure, the grease forms a thin layer and reduces friction through its own lubricity [11–13].

At present, spherical hinge lubrication of a rotary bridge mainly depends on self-lubrication of sliding block and grease, but there is little research on spherical hinge grease. In engineering, PTFE is usually added to butter and applied between ball joints, but there is no clear specification for the dosage of PTFE, and it is usually added according to experience. If too little is added, it will fail to achieve lubrication effect; on the contrary, if too much is added, it may lose its lubrication effect due to agglomeration [14].

With the continuous leaps in science and the continuous development of industrialization, the demand for grease is also increasing year by year, and the quality requirements are becoming higher and higher [15,16]. Excellent lubrication technology can reduce energy loss, increase the service life of equipment and reduce production costs. Grease is composed of base oil, thickener and additives [17–19]. The additives can change the working mechanism and performance of grease, and have a total impact on lubrication effect, wear reduction and antiwear [20,21]. Since the beginning of the new century, nanomaterials have been used as additives in grease. Studies show that the addition of nanoparticles can effectively improve the friction and wear properties [22–26].

At present, self-lubricating ceramic materials are widely used in the field of cutting tools. There are wide applications for metal matrix nanocomposites in smart materials, biomedical devices, energy storage and electronic devices and other tribology-related fields. Self-lubricating materials are becoming more and more common in fields such as metal forming or power generation. At the same time, with the increasing tonnage of rotary bridges, the demand for rotation is increasing day by day. PTFE powder cannot meet these demands, and thus, it is necessary to improve the self-lubrication performance of lubricating materials [27–30]. A season frozen region of bridge construction and other differences requires a long cycle across a bad environment due to large temperature differences. The spherical hinge may have issues with grease due to water erosion. Water vapor in temperature under the action of the freeze–thaw phenomenon may produce degradation of lubricating material under freeze–thaw cycles, and even complete failure. Its status in the globe hinge structure is completely unknown. This issue also increases the risk of the bridge turning. In order to solve this problem, it is necessary to ensure that the grease has good frost resistance.

To sum up, three lubrication additives—graphene, carbon nanotubes (CNTs) and tungsten disulfide (WS_2)—were selected as replacement materials for friction and wear test and a shear rheological test. The tribological properties and rheological properties of grease mixed with several additives were tested at room temperature and two states after freeze–thawing so as to find the grease additive with the best comprehensive performance [31–39]. This work can provide guidance for the selection of spherical hinge lubrication materials in the future.

2. Materials and Sample Preparation

2.1. Base Grease

The basic grease used in this paper is lithium base grease produced by Sinopec Lubricating Oil Company, and its properties are shown in Table 1.

Table 1. Properties of base grease.

Lithium Base Grease	Base Oil	Tickener	Vscosity	Cnsistency
Index number	PAO	Lithium 12 hydroxyl stearate	32 mm^2/s	275–285

2.2. Lubricating Additive

The nanoscale PTFE powder used in this paper is produced by Ford Plastics Co., LTD. (Mianyang, China), graphene and CNTs are produced by Wuhan, Hubei, China Hong da chang Evolution Technology Co., LTD., and WS_2 is produced by Hua jing Powder Materials Co., LTD. (Changsha, China). The main performance indexes are shown in Table 2.

Table 2. Lubrication additive properties.

Serial Number	1	2	3	4
PTFE	Moisture Content	Average Particle Size D50	Apparent Density	Decomposition Temperature
Unit	N/A	mm	g/L	°C
Index Number	≤0.05%	1.6 ± 0.6	≤450	360
Gaphene	Particle size D50	Granularity D90	Single rate	Thickness
Unit	um	um	N/A	layer
Index Number	7–12	11–15	>80%	1–3
CNTs	NH2 content	Specific surface area	Atual density	Peparation methods
Unit	wt%	m^2/g	g/cm^3	N/A
Index Number	0.45	>233	2.1	CVD
WS_2	Color	Particle size	Specific surface area	Prity
Unit	N/A	Mm	m^2/g	N/A
Index Number	Back	≤100	10.506	≥99.9%

2.3. Preparation of Lubricating Materials

First, 50 g base and lubricating grease is added into the beaker, considering the best dosage of additives. More mixing ratio design groups are used in order to ensure the powder dispersion is good. At the same time, we aim to join T154 polyisobutylene butadiene imide dispersant properties, as shown in Table 3. They are mixed evenly in three roller grinding machines 4 times to get even samples of grease. Figure 1 shows the grease that has been configured.

Table 3. Properties of T154 polyisobutene–diene imide raw materials.

Poject	Dnsity	Flash Point	Kinematic Viscosity	Water Content
Unit	kg/m^3	°C	mm^2/s	N/A
T154	1920	180	140	≤0.08%

In order to consider the performance changes of lubricating materials in the freezing–thawing environment, 5% of the mass fraction of water is mixed into the grease, evenly stirred in an environment of −25 °C for 24 h, and then put in an environment of 25 °C for 24 h to complete a freezing–thawing cycle. In this experiment, a total of 11 groups of freeze–thaw cycles are conducted, and samples with different freeze–thaw cycles are obtained.

Figure 1. Grease with different additives.

3. Methods

3.1. Test of Friction Coefficient

At present, the determination of the friction force at the spherical hinge interface of the horizontal rotary body is mainly based on the combination of theoretical calculation and field measurement, and there is still no laboratory test of the friction force at the spherical hinge interface of the horizontal rotary body. The research group developed a device for measuring the friction of an indoor horizontal rotary spherical hinge interface, including spherical hinge structure, a load system and a traction system.

The equipment treats the entire rotation body as a rigid body, and exerts the rotational torque, rotating the body to ensure rigid body rotation around the spherical hinge. When the rotating body transitions from stationary state into the friction state, rotational displacement mutation occurs, applying the rotation of the rotating body and the static friction torque to create an unbalanced torque moment at the moment of balance during a critical state of action. According to the static equilibrium equation, the unbalance moment of the rotating body can be obtained, the mathematical model of the friction moment of the spherical hinge is established and the formulas of the friction moment and the static friction coefficient are derived.

The traction system developed by the device can ensure that the forces on both sides of the upper spherical hinge structure are always equal and opposite, effectively avoid the generation of the lateral forces on the spherical hinge and more accurately simulate the actual requirements of the turning process of the horizontal rotating bridge to ensure that the test results are true and accurate. The equipment sets four angle adjustment fixed pulleys, and the four angle adjustment fixed pulleys (fixed pulley), traction pulley (dynamic pulley) and slide are installed on the outside of the spherical hinge structure. They are used to change the direction of force transmission, reduce traction loss and ensure that the spherical hinge maintains stable speed in the process of rotating with balanced and stable force.

The equipment is tested according to the following steps:

Figure 2 shows the measuring device for friction resistance at the spherical hinge interface. The lubricating oil is smeared evenly on the surface of the lower spherical hinge until it is completely covered and then completely fit to the upper and lower spherical hinge. The upper spherical hinge is slowly rotated to squeeze out the bubbles between the plates so that the lubricating oil is evenly coated.

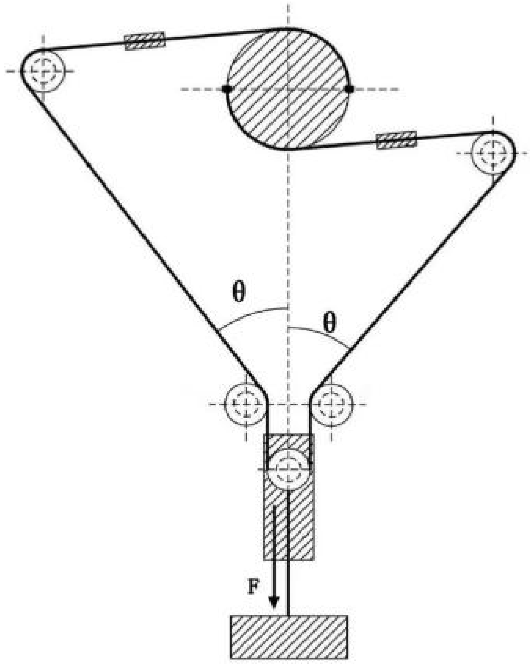

Figure 2. Measuring device for friction resistance at spherical hinge interface.

According to the weight of the bridge set, the number of dead weights is fast (0–200 N). According to the set turning speed, the tractor is started and we record the data of the two electronic digital display tension tables on both sides of the upper spherical hinge structure.

According to the collected traction force and the total weight of the bridge body above the spherical hinge, the friction coefficient of the spherical hinge interface can be calculated according to Equation (1). Each group of experiments is conducted five times to take an average.

$$\mu = 3\frac{F}{W} \tag{1}$$

μ: Friction coefficient of spherical hinge interface.
F: Traction.
W: Total weight of the bridge above spherical hinge.

3.2. Friction and Wear Experiment

The test instrument used in this paper is the MRS10 four-ball testing machine produced by Tian hong Yi hua Electromechanical Co., LTD. (Suzhou, China). In the experiment, the role of three steel bearing balls is fixed. Grease filling daub is fixed at the top of the ball and the center axis through the transmission of load. A friction pair forms between three balls under the first ball and subjected to a test temperature, steel ball speed and load size settings that will eventually wear on the surface of the steel ball and affect the running state of the steel ball. This is carried out to determine the antiwear performance of grease. Each experiment is repeated three times, and the average value of the three experiments is taken. The friction pair is cleaned with petroleum ether before and after each experiment. According to the standard SH/T0204, wear scar diameter (WSD) and average friction coefficient are obtained. According to the standard SH/T0202, maximum non-clamping load (PB) value and wear mark diameter are obtained.

3.3. Shear Rheological Test

In this paper, a MCR302 rheometer is used to test the rheological properties of grease. The thixotropic performance is tested in the rotating mode of plates with spacing of 1 mm. The test method is as follows: The shear rate gradually increases from 0.01 s^{-1} to 500 s^{-1}, and after constant shearing, the shear rate gradually decreases from 500 s^{-1} to 0.01 s^{-1}. The apparent viscosity test is conducted in cone–plate mode. In order to ensure the uniformity of sample temperature, preshear treatment is carried out for 1 min before the test with a preshear rate of 100 s^{-1}, test spacing of 0.1 mm, test shear rate of 1000 s^{-1} and test time of 5 min. Each group of experiments is repeated at least three times.

4. Results and Discussion

4.1. Tribological Properties

4.1.1. Determination of the Optimal Dosage of Spherical Hinge Grease Additive

The friction coefficient of grease was measured by a self-developed measuring device with a spherical hinge friction coefficient, and the optimal dosage of lubricant additive was obtained via quadratic curve fitting.

It can be seen from Table 4 that the friction coefficients of the four additives all have roughly the same variation trend, decreasing first and then increasing. This is because when the additive concentration is insufficient, the base oil plays the main lubrication role. When the additive concentration is at the best dosage, the additive is evenly dispersed in the oil film, and the best performance is obtained. When the concentration of additives is too high, additives accumulate in the grease to form abrasive particles, and shear failure occurs in the lubrication domain, leading to an increase in the friction coefficient.

Table 4. Optimum dosage of spherical hinge grease additive.

Species	Dosage	Coefficient of Friction	Fitting Equation	Best Dosage
PTFE	0.1% 0.5% 1.0% 1.5%	0.078 0.072 0.066 0.070	$y = 0.0128x^2 - 0.0268x + 0.081$	1.0%
Graphene	0.05% 0.10% 0.15% 0.20%	0.066 0.051 0.052 0.054	$y = 1.7x^2 - 0.495x + 0.0858$	0.1%
CNTs	0.05% 0.10% 0.15% 0.20%	0.073 0.066 0.081 0.107	$y = 3.3x^2 - 0.591x + 0.0938$	0.1%
WS_2	1.0% 1.5% 2.0% 2.5%	0.080 0.077 0.060 0.067	$y = 0.01x^2 - 0.0462x + 0.1181$	2.3%

4.1.2. Determination of Friction Coefficient after Freeze–Thaw

According to freeze–thaw method, after 11 freeze–thaw cycles, the friction coefficients of the four additive greases are shown in Figure 3.

It can be seen from Figure 3 that the friction coefficients of the four additives all gradually increase with the increase in freeze–thaw times, PTFE showing the largest increase and WS_2 showing the smallest increase. The friction coefficients of the four additives tend to be stable after seven rounds of freeze–thawing, so the grease after seven rounds of freeze–thawing is used for performance tests in this paper.

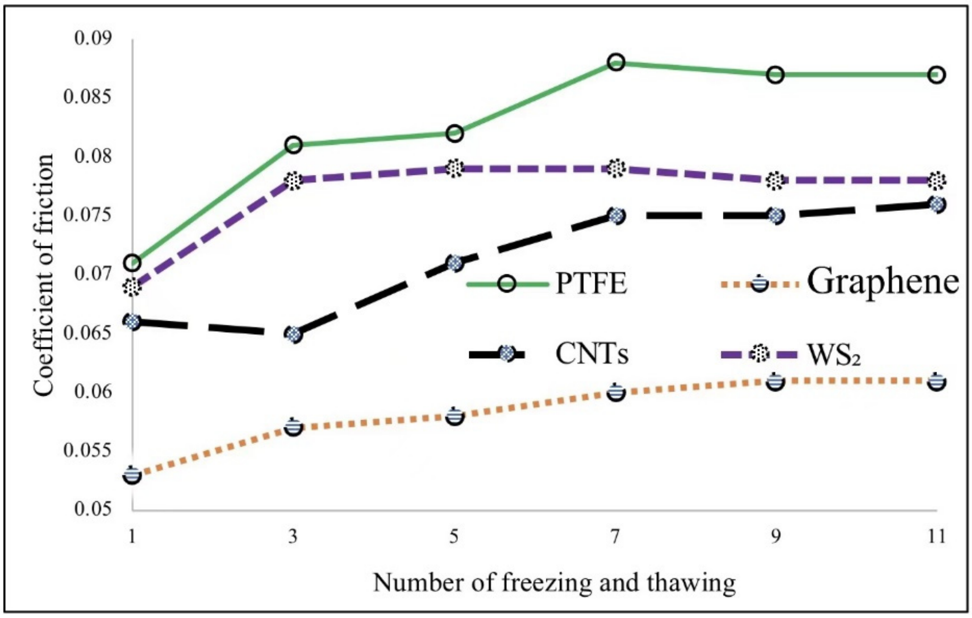

Figure 3. Friction coefficient of grease after freeze–thawing.

4.1.3. Friction and Wear Performance

According to the optimal dosage, four kinds of grease are configured for the four-ball test, and the experimental results are shown in Figure 4.

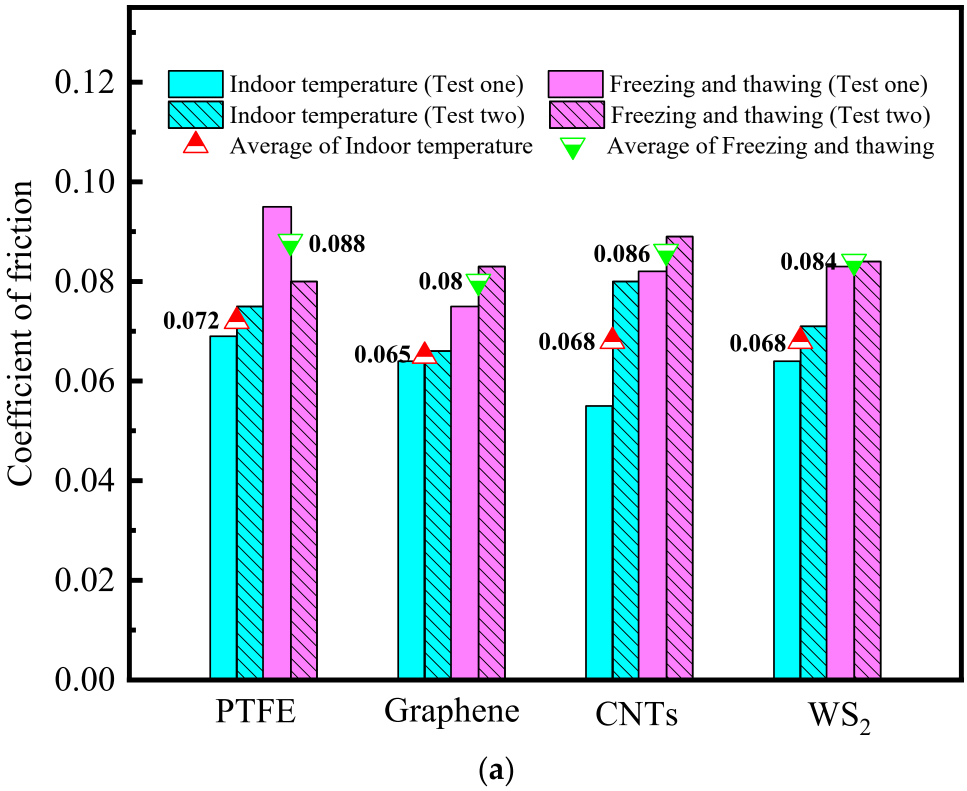

Figure 4. *Cont*.

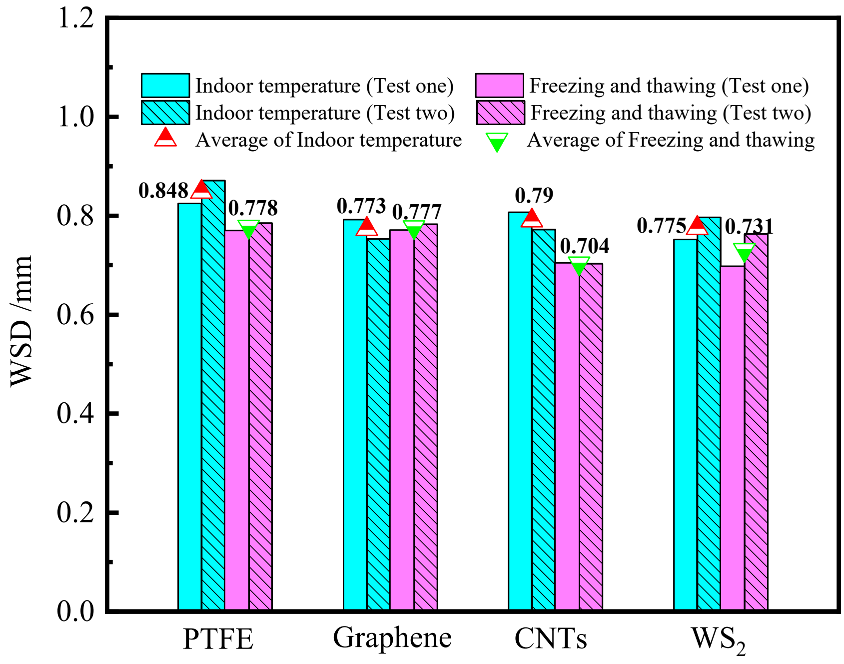

(**b**)

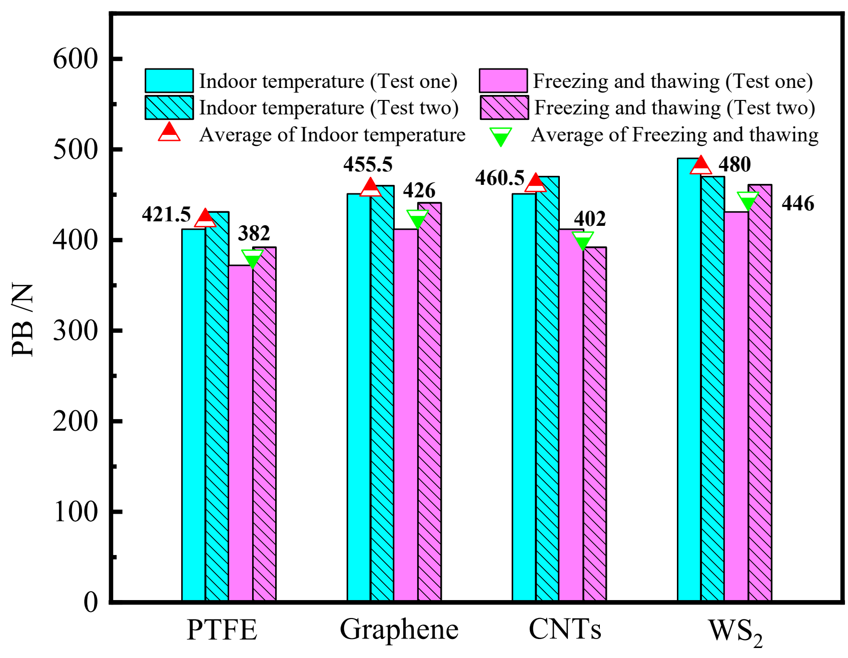

(**c**)

Figure 4. Comparison of tribological properties of admixtures for spherical hinge lubrication: (**a**) COF (**b**) WSD (**c**) PB.

Figure 4 shows that at indoor temperature, the minimum friction coefficient is demonstrated by graphene grease and the maximum is demonstrated by PTFE grease. The minimum WSD is demonstrated by graphene grease and the maximum is demonstrated by PTFE grease. The maximum PB is demonstrated by WS_2 grease, and the minimum is demonstrated by PTFE grease. This shows that the lubricity, wear resistance and bearing capacity of the three substitute materials are better than that of PTFE at room temperature, and graphene is the best in comprehensive performance. After freeze–thawing, the minimum friction coefficient is that of graphene grease, and the maximum is that of

PTFE grease. The minimum WSD is that of CNTs grease; the maximum is that of PTFE grease. The maximum PB is that of WS_2 grease, and the minimum is that of PTFE grease. The tribological properties of the three replacement materials after freezing and thawing are also better than that of PTFE, and the comprehensive properties of WS_2 are the best, followed by those of graphene.

It can be seen from Figures 5 and 6 that the WSD does not change much, but corrosion products can be observed around the wear spot, and this layer of sediment cannot be dissolved by the organic solvent of petroleum ether and ethanol. The analysis shows that because the experimental samples undergo many freeze–thaw, the lubricating grease and water are fully mixed, and under the condition of long-term exposure to the air, the oxidation and deterioration of the oil is promoted, and the olefins in the oil are oxidized into carboxylic acids. Due to the existence of moisture and carboxylic acids, the lubrication film formed by grease is destroyed, leading to wear of the experimental steel ball, making the grease effect worse. At the same time, the carboxylic acids formed by oxidation corrode the metal, resulting in uneven rust spots on the surface of the experimental steel ball, resulting in a rough contact surface and poor wear reduction effect of grease. To sum up, due to these two reasons, corrosion products are generated around the wear spot of the freezing–thawing grease, resulting in greater friction coefficient of the grease after multiple freezing–thawing cycles under the same experimental conditions.

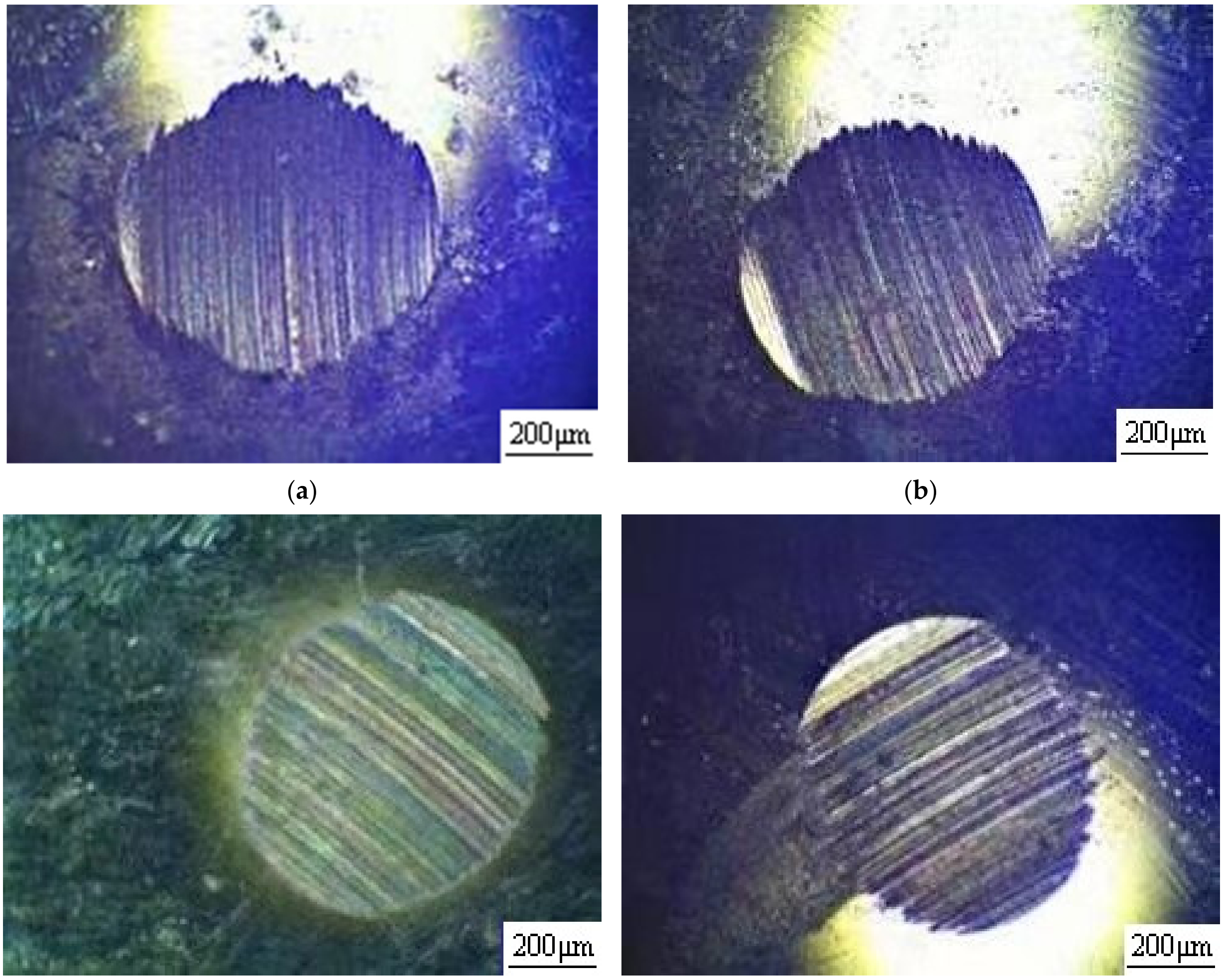

(**a**) (**b**) (**c**) (**d**)

Figure 5. Grease wear marks at room temperature: (**a**) PTFE; (**b**) Graphene; (**c**) CNTs; (**d**) WS_2.

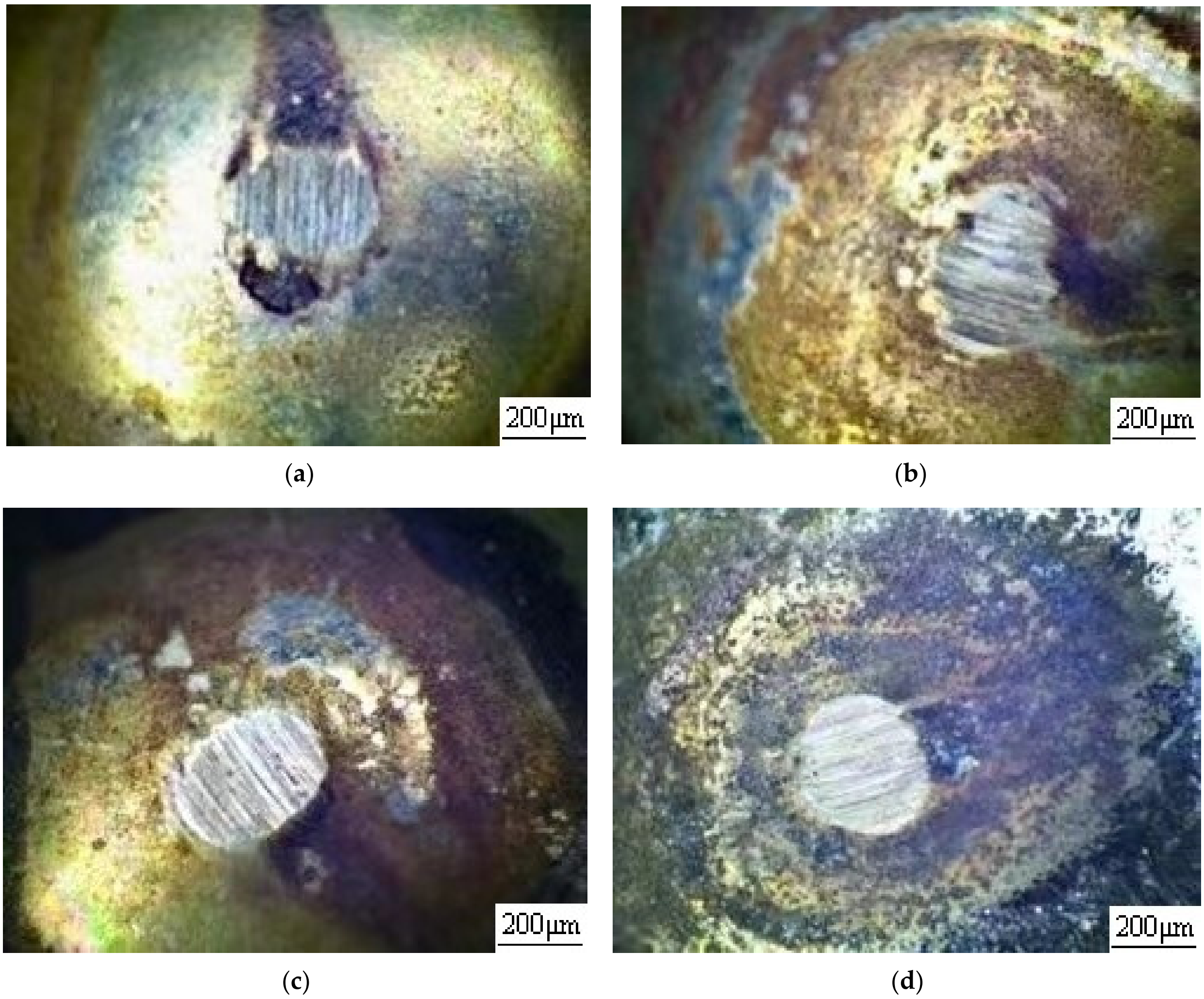

Figure 6. Wear marks of grease after freeze–thaw: (**a**) PTFE; (**b**) Graphene; (**c**) CNTs; (**d**) WS_2.

From the experiment phenomenon and the corresponding data, it can also be concluded that graphene has the minimum friction coefficient of the grease, but the spot diameter is not the lowest. This is because graphene nanoparticles have large surface energy, making it easier for the nanoparticles form larger particle sizes in the process of friction reunion settling. On the one hand, this means they are unable to fully participate in the role of antiwear. On the other hand, it causes extra abrasive wear, making the diameter of the grinding spot larger. This is also the main friction mechanism resulting in the minimum friction coefficient of graphene grease, but not the minimum diameter of the spot.

4.2. Rheological Characterization

4.2.1. Characterization of Thixotropic Properties

Rheology refers to the flow and deformation properties of grease under the action of external forces, including thixotropy, viscoelasticity and apparent viscosity. Under the action of external shear, the hydrogen bonds between the soap fibers are destroyed, and directional rearrangement and stacking are conducted along the shear direction, which decreases the oil fixation ability of the fibers originally crossed into a network structure, resulting in increased oil separation, reduced consistency, and good flow performance. When the external force disappears, the intermolecular interaction forces will make the oriented and arranged soap fibers gather gradually and return to the structure state in which they cross each other. However, the recovery process is not completely reversible, and a small part of the fibers will be cut and destroyed by external forces, which cannot be fully restored to the initial state. This process is the thixotropy of grease, which also represents the characteristics of the grease from static to flow, and the recovery after the external force disappears. Thixotropy is generally used to characterize the thixotropy caused by external force, and the area of the thixotropy ring formed by the above row and downward reciprocating shear curves is used as the evaluation criterion.

The larger the thixotropic ring, the higher the damage rate of grease is than the recovery rate; that is, the worse the recovery of grease. On the contrary, the smaller the thixotropic ring, the better the recovery of grease after damage.

It can be seen from Figure 7 that the maximum thixotropy ring of PTFE grease is 137,207 Pa/s, while the thixotropy ring of the grease containing graphene, WS_2 and CNTs is 81,679 Pa/s, 96,386 Pa/s and 90,194 Pa/s, respectively, with graphene being the smallest. The thixotropy of graphene, WS_2 and CNTs is better than that of PTFE.

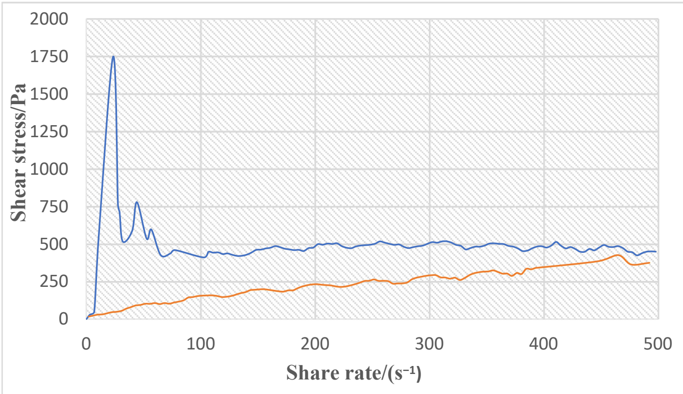

(**a**)

(**b**)

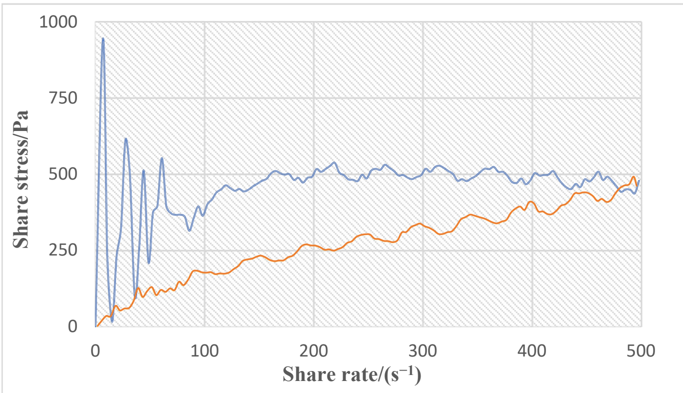

(**c**)

Figure 7. *Cont.*

(**d**)

Figure 7. Lubrication additive thixotropic ring: (**a**) PTFE; (**b**) Graphene; (**c**) CNTs; (**d**) WS_2.

Figure 8 shows that among the four greases, the maximum thixotropic ring of PTFE grease is 110,428 Pa/s and the thixotropic performance is the worst. The thixotropic ring of graphene is 64,878 Pa/s, which has the best thixotropy and recovery. The thixotropic ring areas of CNTs and WS_2 are 99,142 Pa/s and 92,114 Pa/s, which are better than those of PTFE. The minimum thixotropic ring of graphene is due to the large pore volume of graphene. Under the action of high shear force, the base oil absorbed by graphene is more easily released, and the energy required to destroy graphene grease is small. In a certain period of time, the structure of graphene grease recovers faster.

(**a**)

Figure 8. *Cont.*

(**b**)

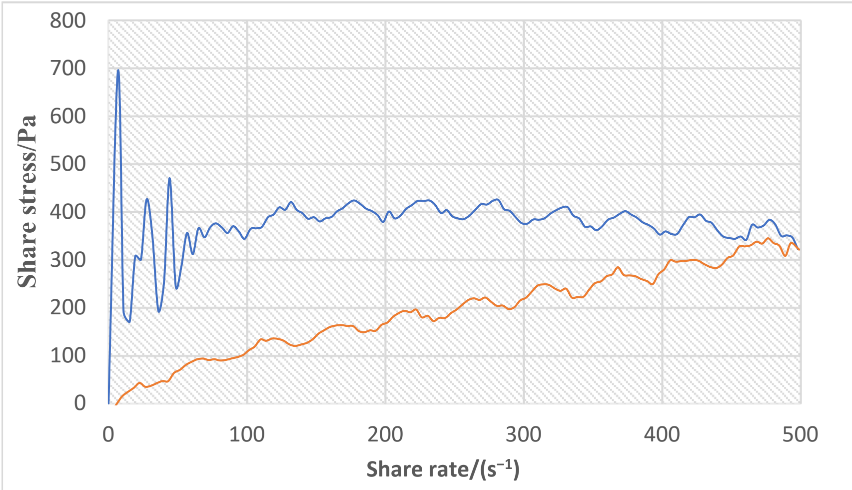

(**c**)

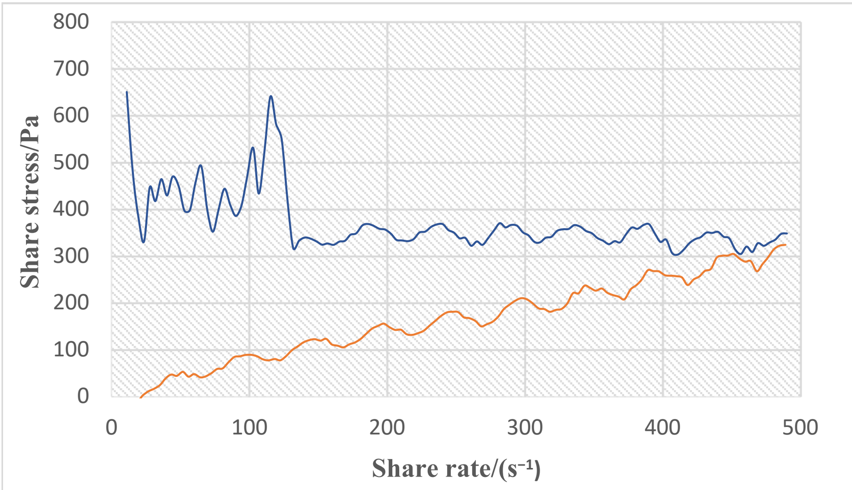

(**d**)

Figure 8. Thixotropic ring after grease freeze–thaw for 7 times: (**a**) PTFE; (**b**) Graphene; (**c**) CNTs; (**d**) WS_2.

4.2.2. Viscoelastic Energy Characterization

Energy storage modulus (G′), which is essentially Young's modulus and the real part of the complex modulus, represents the energy stored by elastic deformation of viscoelastic materials during deformation. It is an index of material rebound after deformation and represents the ability of materials to store elastic deformation energy. The loss modulus (G′′) is also known as the viscous modulus, and the imaginary part of the complex modulus refers to the energy lost due to the viscous deformation (irreversible) when the material is deformed, which reflects the viscosity of the material. When the storage modulus is greater than the loss modulus, the elastic deformation of the grease can be recovered. When the storage modulus is equal to the loss modulus, the grease is semi-solid. When the loss modulus is greater than the storage modulus, the grease will undergo viscosity deformation and has irreversible viscous energy.

It can be seen from Figure 9 that the four materials all enter the non-linear viscoelastic region after experiencing the linear viscoelastic region, and the intersection of the storage modulus and the loss modulus appears to be the phase transition point, where shear stress represents the structural strength of grease. It can be seen from the figure that the intersecting strains of PTFE, graphene, CNTs and WS_2 are 8.9, 12.7, 13.9 and 12.2, respectively. This indicates that PTFE has the lowest structural strength and the worst elastic recovery, while CNTs have the highest structural strength and the best elastic recovery.

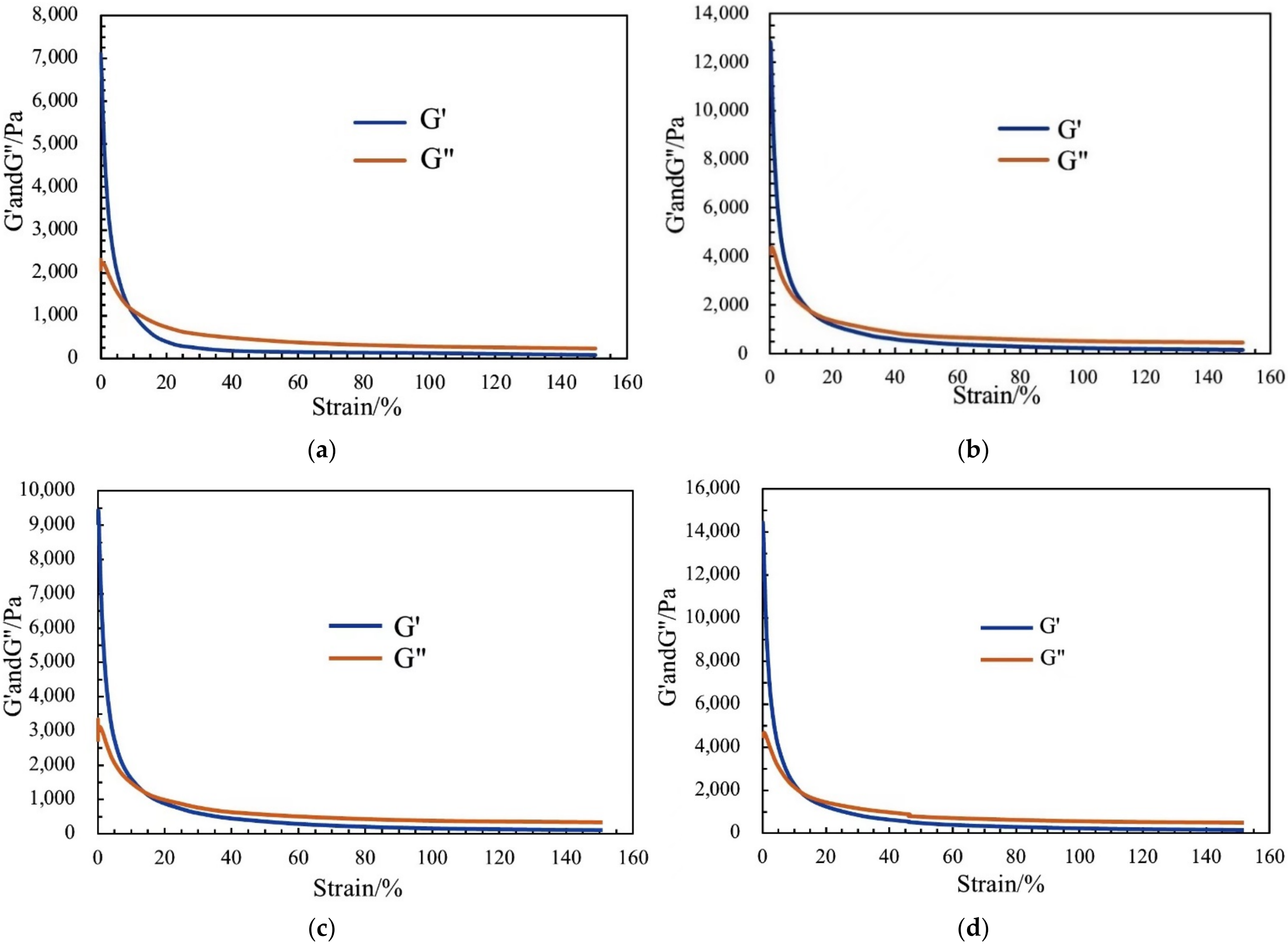

Figure 9. Grease modulus curve: (**a**) PTFE; (**b**) Graphene; (**c**) CNTs; (**d**) WS_2.

As can be seen from Figure 10, after seven freezing and thawing energy-storage loss modulus tests, all four arterials intersect, and the intersection points of polytetrafluoroethylene, graphene, CNTs and WS_2 are at 8.9, 14.6, 12.1 and 14.4, respectively. It can be seen that among the four additives, PTFE has the earliest phase transition point and the worst elastic recovery, while graphene has the best elastic recovery and the largest structural strength. The greater the structure strength of grease, the more difficult grease is to lose.

Even in the vertical direction or without sealing the friction parts, it still can maintain enough thickness, even under the action of centrifugal force, to ensure reliable lubrication. Only high structural strength is suitable for the construction of a rotating bridge. Therefore, the high-strength performance of graphene is most suitable for the construction of rotating bridge grease additive.

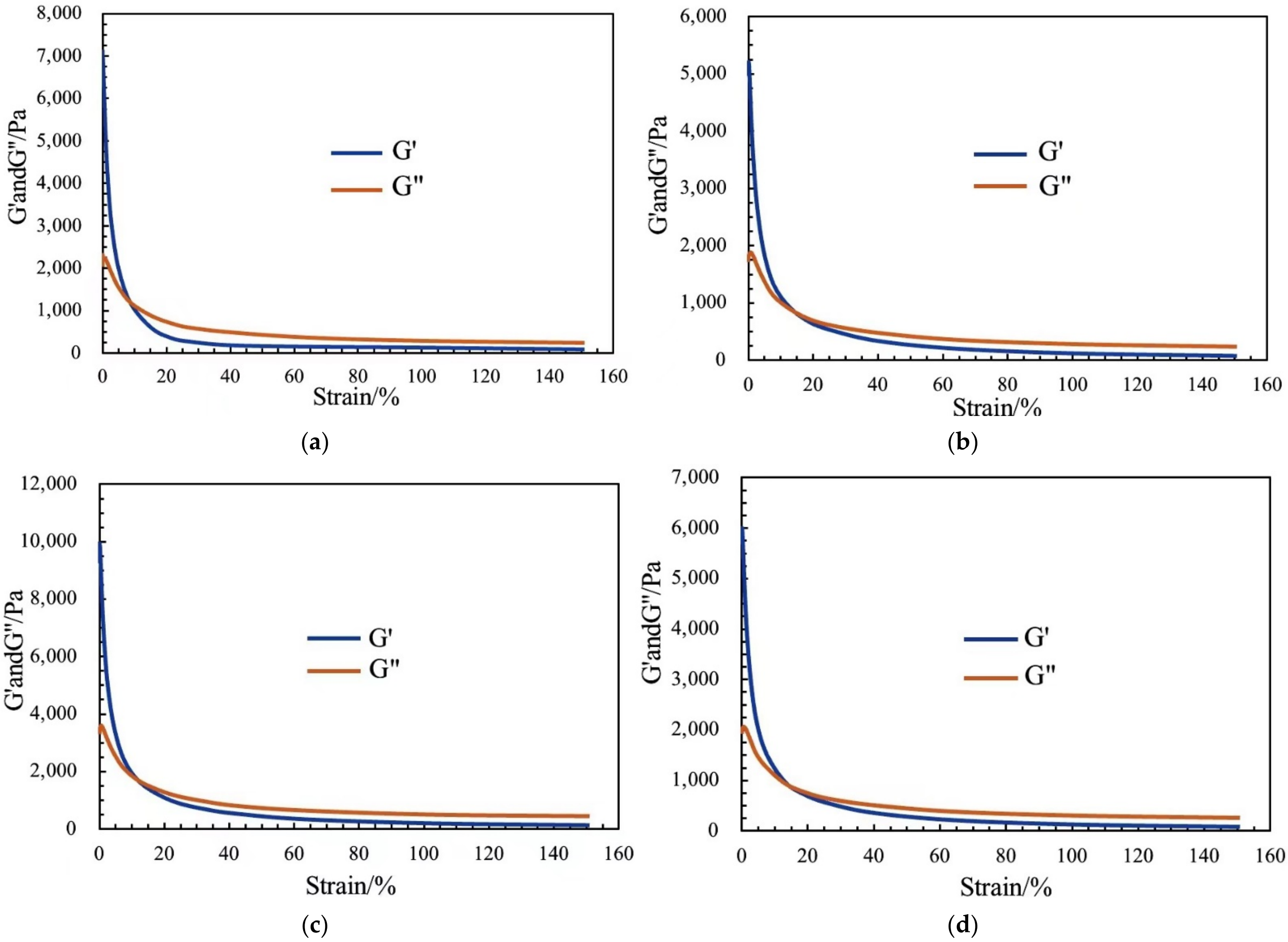

Figure 10. Modulus curve of grease after 7 rounds of freeze–thawing (**a**) PTFE; (**b**) Graphene; (**c**) CNTs; (**d**) WS_2.

The molecules of grease are mainly connected by hydrogen bonds and van der Waals forces to form a stable spatial structure. Different molecular groups form intermolecular forces with different strengths and spatial structures with different strengths. In this paper, the apparent viscosity was used to determine the fluidity of grease. Figure 10 shows the viscosity change curve of grease with PTFE powder, graphene, WS_2 powder and CNTs at constant shear rate at room temperature.

It can be seen from Figure 11 that the viscosity of the four greases decreases significantly with the increase in shear time. At 300 s shear, the viscosity of PTFE grease is 1.67 Pa·s, the viscosity of WS_2 grease is 1.85 Pa·s—10.8% higher than that of PTFE—and the viscosity of graphene grease is 1.78 Pa·s, which is 6.6% higher than that of PTFE. The viscosity of CNTs grease is 1.76 Pa·s, which is 5.4% higher than that of PTFE. This shows that the properties of the three replacement materials are better than that of PTFE, among which WS_2 is the best.

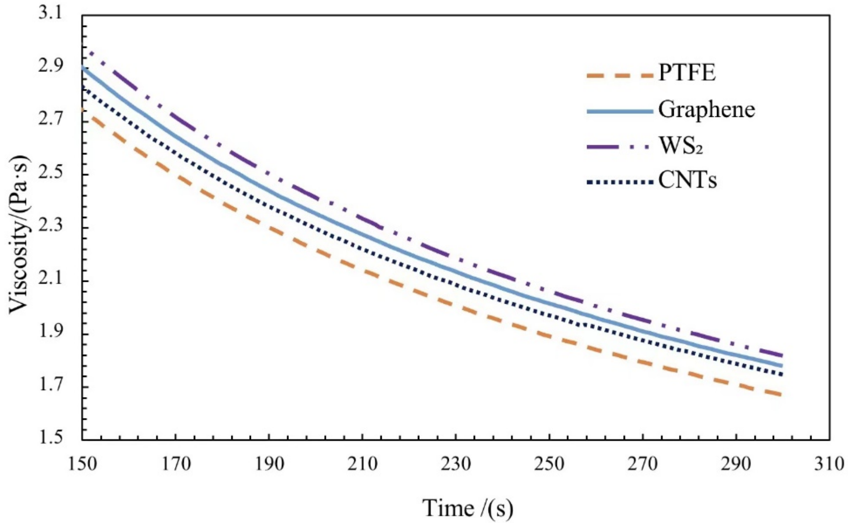

Figure 11. Change of apparent viscosity of grease with time under shear condition.

As can be seen from Figure 12, with the increase in shear time, the apparent viscosity of CNTs greases first increases and then gradually decreases, while the other three greases gradually decrease with the increase in shear time. At 300 s shear, the viscosity of PTFE grease is 1.09 Pa·s, and the minimum viscosity of WS_2 grease is 0.74 Pa·s, 32% lower than PTFE. The maximum viscosity of graphene grease is 1.90 Pa·s, which is 74% higher than that of PTFE. The viscosity of CNTs grease is 1.56 Pa·s, 43% higher than that of PTFE. This indicates that the properties of graphene and CNTs are better than those of PTFE, among which graphene is the best, and WS_2 is inferior to PTFE under freeze–thaw conditions.

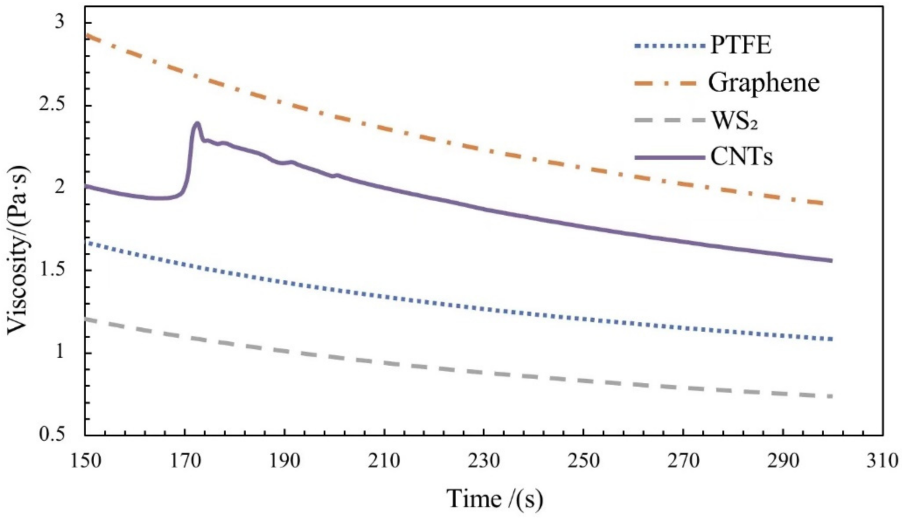

Figure 12. Changes of apparent viscosity with time of various freeze–thaw greases under shear conditions.

The main reason why the apparent viscosity of grease initially decreases with time and then tends to be stable is as follows: grease is a colloidal structure composed of soap fiber and base oil. The apparent viscosity of grease is related to the thin consistency of grease, which in turn is related to the size of soap fiber. The larger the size of soap fiber, the more obvious the shear-thinning phenomenon. Under high-speed shear, the size of soap fiber is constantly reduced, while the size and direction of soap fiber become more and more stable, so the apparent viscosity of grease tends to be constant. The abnormal phenomenon that the apparent viscosity of CNTs first increases and then decreases is due to structural adjustment, and no stable colloidal structure is formed. The experimental results show that graphene grease has better shear resistance and fluidity and is more suitable for harsh construction conditions of rotary bridges.

5. Conclusions

In this paper, the tribological properties and seasonal freezing damage evolution characteristics of a variety of rotating spherical hinge self-lubricating coating materials were studied by means of friction coefficient measurement experiments, friction and wear experiments and shear rheological experiments based on a self-developed indoor spherical hinge rotational friction coefficient tester. The specific conclusions are as follows:

Through friction and wear study and fitting analysis of friction coefficient, the optimal dosages of PTFE, graphene, CNTs and WS_2 were determined to be 1%, 0.1%, 0.1% and 2.3%, respectively.

The friction coefficient of graphene grease is 0.065, 0.007 smaller than PTFE; the diameter of the grinding spot is 0.79 mm, which is 84% of PTFE; the maximum no-stick bite load is 455.5 N, 8.1% higher than PTFE; the thixotropy ring area is 81,679 Pa/s, 41% lower than PTFE; the strain of phase transition point is 12.7, which is higher than PTFE (42%). The apparent viscosity of the grease is 1.78 Pa·s, 6.6% higher than that of PTFE. This shows that graphene has better lubrication effect, bearing capacity, thixotropy and structural strength.

The friction coefficient of graphene grease after freezing and thawing is 0.08 lower than PTFE 0.008, the diameter of wear spot is 0.777 lower than PTFE 0.008, the maximum no-bite load is 426 N, which is 11.5% higher than PTFE, and the thixotropy ring area is 64,878 Pa/s lower than PTFE 42%. The strain at phase transition point 14.6 is 64% higher than that of PTFE, and the apparent viscosity is 1.90 Pa·s, 74% higher than that of PTFE. This shows that graphene can replace PTFE as grease additive, which can effectively reduce spherical hinge friction, and can have its due effect in winter in seasonal freezing areas and adapt to practical construction.

Author Contributions: Conceptualization, W.D.; Data curation, J.Z. and D.L.; Formal analysis, J.Z., X.G. and W.D.; Methodology, D.L. and X.G.; Project administration, W.D.; Writing—original draft, J.Z.; Writing—review and editing, X.G. and W.D. All authors have read and agreed to the published version of the manuscript.

Funding: This study was supported by the National Natural Science Foundation of China (NSFC) (51178204) and the Science and Technology Development Program of Jilin Province (20190303033SF). We are grateful for this financial support.

Institutional Review Board Statement: Not applicable.

Informed Consent Statement: Not applicable.

Data Availability Statement: Not applicable.

Conflicts of Interest: The authors declare that there is no conflict of interest regarding the publication of this paper.

References

1. Yu, F.; Qi, J.; Wang, J.; Zhang, W.; Zhang, Q. Rotation Construction of Heavy Swivel Arch Bridge for High-Speed Railway. *Structures* **2020**, *26*, 755–764. [CrossRef]
2. Zhang, X.D.; Che, X.J. Stability Impact Analysis of Random Dead Load Distribution to T-Rigid Frame Bridge Swivel Construction. *Appl. Mech. Mater.* **2013**, *361–363*, 1348–1352. [CrossRef]
3. Ashiquzzaman, M.; Hui, L.; Ibrahim, A.; Lindquist, W.; Thomson, M.; Hindi, R. Effect of Inconsistent Diaphragms on Exterior Girder Rotation during Overhang Deck Construction. *Structures* **2016**, *8*, 25–34. [CrossRef]
4. Ashiquzzaman, M.; Hui, L.; Ibrahim, A.; Lindquist, W.; Panahshahi, N.; Hindi, R. Exterior girder rotation of skew and non-skew bridges during construction. *Adv. Struct. Eng.* **2020**, *24*, 134–146. [CrossRef]
5. Zhang, J.; El-Diraby, T.E. Constructability Analysis of the Bridge Superstructure Rotation Construction Method in China. *J. Constr. Eng. Manag.* **2006**, *132*, 353–362. [CrossRef]
6. Feng, F.; Lam, D.; Qy, J. Moment resistance and rotation capacity of semi-rigid composite connections with precast hollowcore slabs. *J. Constr. Steel Res.* **2009**, *66*, 452–461. [CrossRef]

7. Fan, X.J.; De, W.C.; Yang, Y.W. Fine-Analysis for the Concrete Upper Rotation Table and Pier of a Bridge Using Rotation Construction Method. *Appl. Mech. Mater.* **2014**, *3489*, 638–640. [CrossRef]
8. Hu, J.; Sun, X.Y.; Jiao, S.J. Monitoring of long-span self-anchored arch bridge con-structed with rotation method. *Appl. Mech. Mater.* **2012**, *178–181*, 1977–1982. [CrossRef]
9. Sheng, S.Q.; Guo, X.G.; Zhang, d.; Guan, X.K.; Zheng, Y. Research on the Application of Horizontal Rotation Construction Method with Flat Hinge in Cable-Stayed Bridge Construction. *Adv. Mater. Res.* **2011**, *1279*, 255–260. [CrossRef]
10. Xiao, J.; Liu, M.; Zhong, T.; Fu, G. Seismic performance analysis of concrete-filled steel tubular single pylon cable-stayed bridge with swivel construction. *IOP Conf. Ser. Earth Environ. Sci.* **2019**, *218*, 12087. [CrossRef]
11. Temizer, İ.; Bünyamin, E. Investigation on the Combustion Characteristics and Lubrication of Biodiesel and Diesel Fuel used in a Diesel Engine. *Fuel* **2020**, *278*, 118363. [CrossRef]
12. Nor, H.N.N.; Ghani, J.A.; Ramli, R.; Haron, C.H.C. A review on recent development of minimum quantity lubrication for sustainable machining. *J. Clean. Prod.* **2020**, *268*, 122165. [CrossRef]
13. Josep, F.L.; Westerberg, L.G.; Jasmina, C.T.; Johan, L.; René, W. On the Flow Dynamics of Polymer Greases. *Lubricants* **2022**, *10*, 66. [CrossRef]
14. Bai, L.; Chen, Y.; Yin, H.Y.; Sui, X.; Wu, D.; Feng, Y. Insights into the stability of polytetrafluoroethylene aqueous dispersion: Role of surfactant. *J. Mol. Liq.* **2020**, *314*, 113662. [CrossRef]
15. Fabian, K.; Michael, S.; Marcus, K.; Matthias, O. Influence of Lubrication Systems on the Fatigue Strength of Bolted Joints. *Appl. Sci.* **2022**, *12*, 2778. [CrossRef]
16. Anand, A.; Sharma, S.M. High temperature friction and wear characteristics of Fe-Cu-C based self-lubricating material. *Trans. Indian Inst. Met.* **2017**, *70*, 2641–2650. [CrossRef]
17. Mota, V.; Ferreira, L.A. Influence of grease composition on rolling contact wear: Experimental study. *Tribol. Int.* **2009**, *42*, 569–574. [CrossRef]
18. Couronné, I.D.P.N.; Vergne, P.; Mazuyer, D.; Truong-Dinh, N.; Girodin, D. Effects of grease composition and structure on film thickness in rolling contact. *Tribol. Trans.* **2003**, *1*, 31–36. [CrossRef]
19. Delgado, M.A.; Franco, J.M.; Kuhn, E. Effect of rheological behaviour of lithium grease on the friction process. *Ind. Lubr. Tribol.* **2008**, *60*, 37–45. [CrossRef]
20. Emanuela, L.F.; Camilla, M.; Fabio, L.; Patrizia, F. Improvement of Paper Resistance against Moisture and Oil by Coating with Poly(-3-hydroxybutyrate-co-3-hydroxyvalerate) (PHBV) and Polycaprolactone (PCL). *Appl. Sci.* **2021**, *11*, 8058. [CrossRef]
21. Acar, N.; Franco, J.M.; Kuhn, E.; Gonçalves, D.E.P.; Seabra, J.H.O. Tribological Investigation on the Friction and Wear Behaviors of Biogenic Lubricating Greases in Steel–Steel Contact. *Appl. Sci.* **2020**, *10*, 1477. [CrossRef]
22. Patel, J.; Kiani, A. Tribological Capabilities of Graphene and Titanium Dioxide Nano Additives in Solid and Liquid Base Lubricants. *Appl. Sci.* **2019**, *9*, 1629. [CrossRef]
23. Wang, Y.S.; Zhang, P.; Lin, J.H.; Gao, X.D. Rheological and Tribological Properties of Lithium Grease and Polyurea Grease with Different Consistencies. *Coatings* **2022**, *12*, 527. [CrossRef]
24. Huang, Z.; Zhu, J.; Hu, Y.; Zhu, Y.; Zhu, G.; Hu, L.; Zi, Y.; Huang, W. Tin Oxide (SnO_2) Nanoparticles: Facile Fabrication, Characterization, and Application in UV Photodetectors. *Nanomaterials* **2022**, *12*, 632. [CrossRef]
25. Łukasz, M.; Zuzanna, B.; Antoni, R. Rheological Properties of Engine Oil with Nano-Additives Based on MoS2 Materials. *Nanomaterials* **2022**, *12*, 581. [CrossRef]
26. Sun, X.F.; Qiao, Y.L.; Song, W.; Ma, S.N.; Hu, C.H. High Temperature Tribological Properties of Modified Nano-diamond Additive in Lubricating Oil. *Phys. Procedia* **2013**, *50*, 343–347. [CrossRef]
27. Pan, S.; Jin, K.; Wang, T.; Zhang, Z.; Zheng, L.; Umehara, N. Metal matrix nanocomposites in tribology: Manufacturing, performance, and mechanisms. *Friction* **2022**. [CrossRef]
28. Akhtar, S.S. A critical review on self-lubricating ceramic-composite cutting tools. *Ceram. Int.* **2021**, *47*, 20745–20767. [CrossRef]
29. Torres, H.; Rodríguez Ripoll, M.; Prakash, B. Tribological behaviour of self-lubricating materials at high temperatures. *Int. Mater. Rev.* **2018**, *63*, 309–340. [CrossRef]
30. Zhang, Z.; Li, Z.; Pan, S.; Chai, X. Enhanced Strength and High-Temperature Wear Resistance of Ti6Al4V Alloy Fabricated by Laser Solid Forming. *J. Manuf. Sci. Eng.* **2022**, *144*, 111011. [CrossRef]
31. Kałużny, J.; Waligorski, M.; Szymański, G.M.; Merkisz, J.; Różański, J.; Nowicki, M.; al Karawi, M.; Kempa, K. Reducing friction an engine vibrations with trace amounts of carbon nanotubes in the lubricating oil. *Tribol. Int.* **2020**, *151*, 106484. [CrossRef]
32. Srinivas, V.; Rao, C.R.; Rao, N. Lubricating and physico—Chemical properties of CI-4 plus engine oil dispersed with surface modified multi-walled carbon nanotubes. *Tribol.-Mater. Surf. Interfaces* **2018**, *12*, 107–114. [CrossRef]
33. Wang, F.F.; Feng, L.J.; Lu, M. Mechanical Properties of Multi-Walled Carbon Nanotube/Waterborne Polyurethane Conductive Coatings Prepared by Electrostatic Spraying. *Polymers* **2019**, *11*, 714. [CrossRef] [PubMed]
34. Shirasu, K.; Miyaura, T.; Yamamoto, G.; Suzuki, T.; Naito, K.; Hashida, T. Enhanced tribological performance of alumina composites reinforced with acid-treated carbon nanotubes under water lubrication. *Diam. Relat. Mater.* **2020**, *101*, 107657. [CrossRef]
35. Ye, X.Y.; Songfeng, E.; Fan, M.J. The influences of functionalized carbon nanotubes as lubricating additives: Length and diameter. *Diam. Relat. Mater.* **2019**, *100*, 107548. [CrossRef]

36. Károly, Z.; Kalácska, G.; Sukumaran, J.; Fauconnier, D.; Kalácska, Á.; Mohai, M.; Klébert, S. Effect of Atmospheric Cold Plasma Treatment on the Adhesion and Tribological Properties of Polyamide 66 and Poly(Tetrafluoroethylene). *Materials* **2019**, *12*, 658. [CrossRef]
37. Wang, X.B.; Zhang, Y.F.; Yin, Z.W.; Su, Y.; Zhang, Y.; Cao, J. Experimental research on tribological properties of liquid phase exfoliated graphene as an additive in SAE 10W-30 lubricating oil. *Tribol. Int.* **2019**, *135*, 29–37. [CrossRef]
38. Rawat, S.S.; Harsha, A.P.; Chouhan, A.; Khatri, O.P. Effect of Graphene-Based Nanoadditives on the Tribological and Rheological Performance of Paraffin Grease. *J. Mater. Eng. Perform.* **2020**, *29*, 2235–2247. [CrossRef]
39. Jiang, B.; Zhao, Z.; Gong, Z.; Wang, D.; Yu, G.; Zhang, J. Superlubricity of metal-metal interface enabled by graphene and MoWS 4 nanosheets. *Appl. Surf. Sci.* **2020**, *520*, 146303. [CrossRef]